Eur. Phys. J. B **25**, 191–201 (2002)
DOI: 10.1140/epjb/e20020021

THE EUROPEAN PHYSICAL JOURNAL B
EDP Sciences

Orbital-selective Mott-insulator transition in $Ca_{2-x}Sr_xRuO_4$

V.I. Anisimov[1], I.A. Nekrasov[1], D.E. Kondakov[1], T.M. Rice[2], and M. Sigrist[2,3,a]

[1] Institute of Metal Physics, Russian Academy of Sciences-Ural Division, 620219 Yekaterinburg GSP-170, Russia
[2] Theoretische Physik , ETH-Hönggerberg 8093 Zürich, Switzerland
[3] Yukawa Institute for Theoretical Physics, Kyoto University, Kyoto 606-8502, Japan

Received 27 July 2001

Abstract. The electronic structures of the metallic and insulating phases of the alloy series $Ca_{2-x}Sr_xRuO_4$ ($0 \leq x \leq 2$) are calculated using LDA, LDA+U and Dynamical Mean-Field Approximation methods. In the end members the groundstate respectively is an orbitally non-degenerate antiferromagnetic insulator ($x = 0$) and a good metal ($x = 2$). For $x > 0.5$ the observed Curie-Weiss paramagnetic metallic state which possesses a local moment with the unexpected spin $S = 1/2$, is explained by the coexistence of localized and itinerant Ru-4*d*-orbitals. For $0.2 < x < 0.5$ we propose a state with partial orbital and spin ordering. An effective model for the localized orbital and spin degrees of freedom is discussed. The metal-insulator transition at $x = 0.2$ is attributed to a switch in the orbital occupation associated with a structural change of the crystal.

PACS. 75.30.-m Intrinsic properties of magnetically ordered materials – 75.50.-y Studies of specific magnetic materials

1 Introduction

The discovery of unconventional superconductivity in Sr_2RuO_4 [1,2] has evoked considerable interest in the electronic properties of ruthenates. Curiously the substitution of the smaller Ca^{2+}-ions for Sr^{2+}-ions does not lead to a more metallic state but to an antiferromagnetic (AF) Mott insulator with a staggered moment of $S = 1$ as expected for a localized Ru^{4+}-ion which has 4 electrons in the t_{2g}-subshell. As will be discussed below, this insulating behavior is driven by a crystallographic distortion and a subsequent narrowing of the Ru-4*d* bands. The complete series of isoelectronic alloys for intermediate concentrations has recently been synthesized and studied by Nakatsuji and Maeno [3,4]. This gives a rare opportunity to examine the evolution of the electronic structure from a multi-band metal to a Mott-insulator transition in an isoelectronic system. The evolution is not at all monotonic and the metal-insulator transition does not take place as a simple Mott transition but proceeds through a series of intermediate regions with unexpected behavior.

The most dramatic example is the system at a concentration $x = x_c = 0.5$. At this critical concentration the susceptibility shows a free Curie form with a $S = 1/2$ moment (not $S = 1$) per Ru-ion coexisting with metallic transport properties. This critical concentration represents the boundary of the paramagnetic metallic region which evolves as Ca is substituted in the good metal, Sr_2RuO_4. At higher Ca concentrations ($x_c > x > 0.2$), the alloys enter a region with AF correlations at low temperature but still with metallic properties. Insulating behavior appears only at smaller values of $x < 0.2$. The challenge that we address in this paper, is to understand this unexpected and nonmonotonic evolution and in particular the exotic behavior in the vicinity of the critical concentration at $x \approx x_c$.

We begin by discussing the end members. Sr_2RuO_4 is a good metal. Its Fermi surface has been determined by de Haas-van Alphen experiments [7] and agrees very well with the predictions of the local density approximation (LDA) in the density functional theory [8]. Ca_2RuO_4 is a AF Mott insulator and it can be well described by augmenting the LDA by a mean field to include the onsite correlation — the so-called LDA+U method [9]. The third section of this paper is devoted to the examination of the intermediate concentrations by performing calculations for a series of characteristic x-values. The most challenging is the region $x \approx x_c = 0.5$ where there are strong correlations but no symmetry breaking so that both LDA and LDA+U are inapplicable. At this concentration we employ the recently developed *ab initio* computational scheme combining local density approximation and dynamical mean field theory [10–12] (LDA+DMFT) [13,14]. We use LDA calculations to determine the input parameters in the effective Anderson impurity model which in turn is treated using a non-crossing approximation (NCA) [15]. These calculational schemes give us reliable information on the evolution of the electronic distribution among the 3 orbitals in

[a] e-mail: sigrist@itp.phys.ethz.ch

Table 1. Crystallographic data, which is used for LDA calculations: symmetry group, parameters of lattice, atomic positions and distance between nearest atoms. Symbol "/"denotes that for this structure corresponding parameter do not exist.

Compound	Sr_2RuO_4	$Ca_{1.5}Sr_{0.5}RuO_4$	$Ca_{1.8}Sr_{0.2}RuO_4$	Ca_2RuO_4
Symmetry group	I4/mmm	$I4_1/acd$	$P2_1/c$	Pbca
a [Å]	3.8603	5.3195(1)	5.3338(4)	5.6323(3)
b [Å]	3.8603	5.3195(1)	5.3162(4)	11.7463(5)
c [Å]	12.729	25.1734(5)	12.4143(8)	5.3877(2)
Vol. [Å^3]	189.69	712.33(2)	352.01(4)	356.45
β [^{o}]	/	/	90.06(1)	/
Ca(Sr) x	0.0	0.0	0.0141(21)/0.4903(24)	0.0593(4)
Ca(Sr) y	0.0	0.25	0.0137(23)/0.5273(23)	0.3525(2)
Ca(Sr) z	0.14684	0.5492(1)	0.3483(2)	0.0021(5)
O1 x	0.0	0.1933(2)	0.1939(6)	0.3005(4)
O1 y	0.0	0.4433(2)	0.3079(6)	0.0272(2)
O1 z	0.3381	0.125	0.0/0.0196(5)	0.1952(4)
O2 x	0.5	0	−0.0344(5)	−0.0212(4)
O2 y	0.0	0.25	−0.0064(7)	0.1645(2)
O2 z	0.0	0.4568(1)	0.1649(2)	−0.0692(3)
Ru − O1 [Å]	1.930	1.929(1)	1.936(3)/1.926(3)	2.015(2)
			1.941(3)/1.952(3)	2.018(2)
Ru − O2 [Å]	2.061	2.059(3)	2.056(3)/2.056(3)	1.972(2)
Ca − O1 [Å]	2.692	2.399(2)	2.316(7)/2.286(10)	2.292(3)
		2.994(2)	2.445(8)/2.502(9)	2.433(3)
			2.838(11)/2.934(10)	2.565(3)
			3.141(10)/3.037(10)	3.313(3)
Ca − O2 [Å]	2.439	2.326(4)	2.294(4)/2.296(4)	2.287(3)
	2.737	2.664(1)	2.416(12)/2.488(13)	2.362(3)
			2.559(13)/2.444(13)	2.399(3)
			2.772(13)/2.845(13)	3.118(3)
			2.932(12)/2.912(13)	3.296(3)

the t_{2g}-subshell, which we shall show is the key to understanding the electronic properties. The paper concludes with a discussion and summary of our results. A brief account of this work has appeared elsewhere [16].

2 End members: Sr_2RuO_4 and Ca_2RuO_4

We start with Sr_2RuO_4 (or $x = 2$). This is a good metal, forming a 3-dimensional but anisotropic Landau-Fermi liquid at low temperatures [17,18]. Sr_2RuO_4 crystallizes in the undistorted single-layered K_2NiF_4-structure [19,20] (see Fig. 1) with lattice parameters quoted in Table 1. The RuO_6-octahedra are slightly elongated along the c-axis. The Ru-ions have a formal valence Ru^{4+} and have a tetragonal local symmetry. The $2p$-O levels are completely filled, leaving 4 electrons in t_{2g}-subshell of the $4d$-Ru levels. The crystal field level scheme that would apply for an isolated Ru^{4+}-ion is shown in Figure 2. The upper e_g-shell (not included in this figure) is empty. The splitting between the xy-orbitals and the degenerate $\{xz, yz\}$-orbitals is small. But the xy-orbitals π-hybridize with $2p$-orbitals

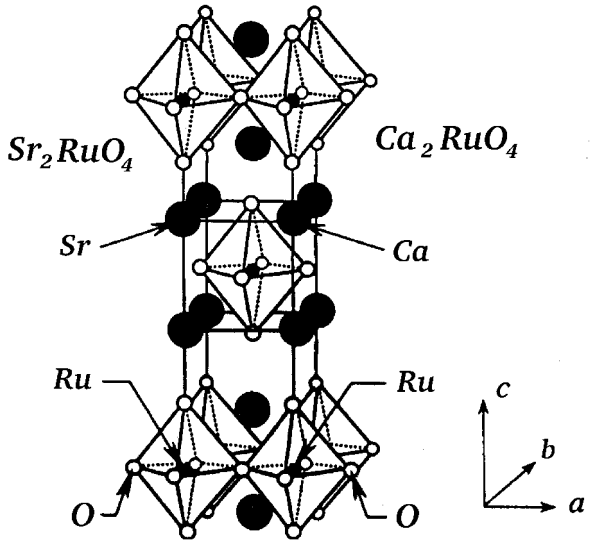

Fig. 1. Basic crystal structure of isoelectronic alloy series $Ca_{2-x}Sr_xRuO_4$.

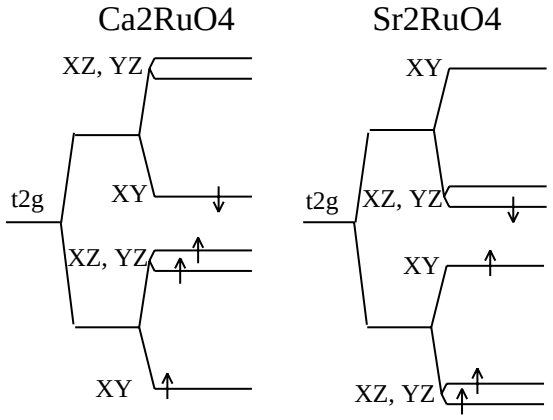

Fig. 2. Local electronic structure of isoelectronic alloy series $Ca_{2-x}Sr_xRuO_4$. In Ca_2RuO_4 spin-down electron occupies xy-orbital (left panel); In Sr_2RuO_4 spin-down electron occupies xz/yz-orbitals (right panel).

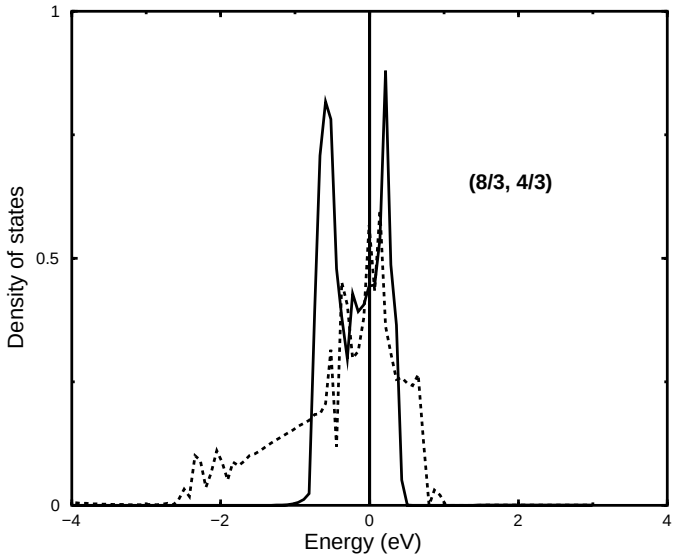

Fig. 3. Density of t_{2g} states for Sr_2RuO_4 obtained from LDA calculation. The solid line is the DOS for the (xz, yz)-orbitals and the dashed line for the xy-orbital. $(n_{(yz,zx)}, n_{xy})$ indicates the electron occupation of the orbitals.

of all 4 in-plane O-neighbors while the $xz(yz)$-orbitals π-hybridize only with the 2 O-neighbors along the $x(y)$-axis. As a result the xy-bandwidth is approximately twice the $\{xz, yz\}$ bandwidth (see Fig. 3). The LDA calculations [8] give 3 Fermi surface sheets, one with essentially xy and two with mixed $\{xz, yz\}$ character. Their shape and volume agree with the de Haas-van Alphen results [7].

The volumes contained by the Fermi surface sheets give an almost equal occupancy of each of the 3 t_{2g}-orbitals. If we denote the occupancy of the $\{xz, yz\}$ and (xy)-orbitals by $(n_{(\alpha,\beta)}, n_\gamma)$, then Sr_2RuO_4 has the fractional occupancy (8/3, 4/3). Although there are clear signs of strong correlations in the enhanced effective mass (enhancements $\sim$3−4 [7,21,22]) and low effective Fermi temperature, the low-temperature behavior is clearly that of a well-defined Landau-Fermi liquid.

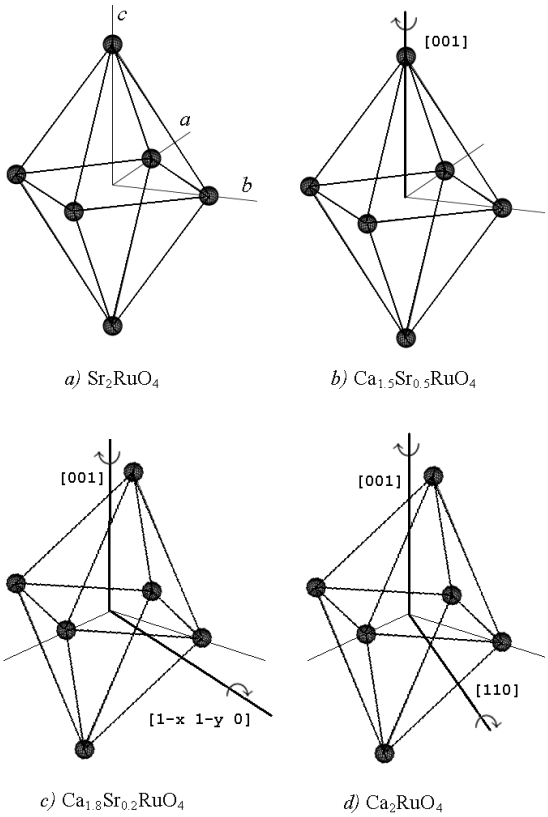

Fig. 4. Scheme of crystal distortion of $Ca_{2-x}Sr_xRuO_4$. Consecutive structural change of the O-octahedra in the alloy series $Ca_{2-x}Sr_xRuO_4$. (a) Ideal structure K_2NiF_4-type (space group I4/mmm); (b) Space group $I4_1/acd$ derives from I4/mmm by rotation around [001]-axis; (c) Space group $P2_1/c$ described by the additional rotation around a free axis in the octahedron basis plane. (d) Space group Pbca derived from the ideal structure by rotation around the [001]- and [110]-axes.

Turning to the other end member, Ca_2RuO_4 or $x = 0$, the substitution of the smaller Ca^{2+}-ion for Sr^{2+} does not lead to a uniform shrinking of the lattice parameter. Instead the RuO_6-octahedra undergo a combined rotation and tilt (Pbca-structure) so that the Ru-O bond length is preserved but the Ru-Ru separation contracts. In Figure 4 we illustrate the relevant distortion of the crystal structure. This distortion bends the Ru-O-Ru bond angle away from 180°, thereby reducing the bandwidth of the t_{2g}-orbitals. Also the smaller size of the Ca^{2+}-ion decreases the interlayer distance (*i.e.* the c-axis lattice constant) which results in a change from elongation to a compression of the RuO_6-octahedra. This in turn changes the sign of the energy splitting between the (xy)- and (xz, yz)-orbitals, so that now the xy-orbital lies lower in energy (see Fig. 2). The crystal structure is orthorhombic (see Tab. 1). All RuO_6-octahedra are equivalent with a rotation around their long axis (0 0 1) and a tilt around the diagonal in-plane axis (1 1 0) (Fig. 4d). Note all inplane O-ions are equivalent in this structure.

Ca_2RuO_4 is an AF insulator. The LDA+U method [9] which is based upon spin-orbital unrestricted Hartree-Fock equation (*i.e.* a static mean field treatment),

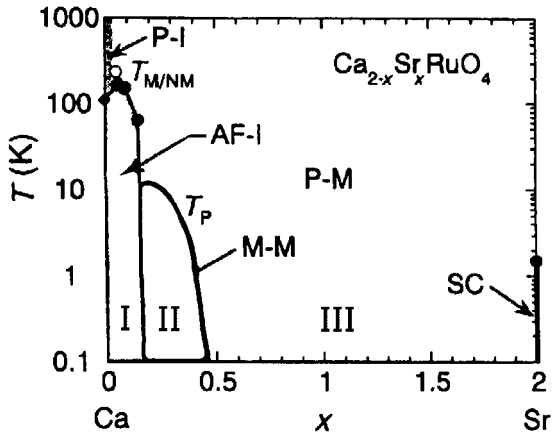

Fig. 5. Phase diagram of $Ca_{2-x}Sr_xRuO_4$. The phases are denoted by the abbreviations P-I for paramagnetic insulating, P-M for paramagnetic metallic, AF-I for antiferromagnetic insulating, AF-M for antiferromagnetic metallic, M-M for magnetic metallic and SC for superconducting (Figure is taken from [3]).

generally works well for magnetic long range ordered insulators [23]. We applied this method to Ca_2RuO_4 choosing parameter values $U = 1.5$ eV and $J = 0.7$ eV for the onsite Coulomb repulsion and the intra-atomic Hund's Rule coupling. The method converged to an AF insulating groundstate in which the lower xy-orbital is fully occupied and the majority spin (xz, yz)-orbitals are also occupied. The sublattice magnetization is reduced by hybridization with the O-orbitals from the full value of 2 μ_B expected for $S = 1$, to 1.35 μ_B. The energy gap is unusually small (0.17 eV). Both these values agree well with experiment, 1.3 μ_B [19] and 0.2 eV [24] respectively. Further treating spin-orbit coupling in second order perturbation theory gives preferred orientation of the magnetic moment along the orthorhombic b-axis (or [1 1 0] in tetragonal notation) also in agreement with experiment [25] (see Appendix).

The LDA+U method gives a satisfactory description of the electronic structure of Ca_2RuO_4. In terms of our previous notation, Ca_2RuO_4 has an integer orbital occupancy of (2,2). The key issue that we address below is the evolution of the electronic structure between these very different end members.

3 Evolution of the electronic structure at intermediate concentrations

The results of our calculations presented above confirm the contrasting behavior of the end members, Sr_2RuO_4 and Ca_2RuO_4. The experimental investigations of Nakatsuji and Maeno show a complex evolution of the electronic structure which they break down into 3 concentration regions, labelled Region I ($0 < x < 0.2$), Region II ($0.2 < x < 0.5$) and Region III ($0.5 < x < 2$), each with its own characteristic behavior. Their results are summarized in the phase diagram (Fig. 5). Below we discuss each of these regions, starting with the Sr-rich region.

3.1 Region III ($2 > x > 0.5$)

The experiments of Nakatsuji and Maeno show that superconductivity is rapidly suppressed when Ca is substituted for Sr in Sr_2RuO_4. This suppression is a natural consequence of disorder for an unconventional superconductor. More interesting is the evolution of the spin susceptibility which progressively increases with Ca substitution and evolves from an enhanced Pauli susceptibility into a Curie-Weiss form. The characteristic (Curie-Weiss) temperature, $\theta_{cw}(< 0)$, approaches zero for $x \to 0.5$. At the same time the linear term in the low-temperature specific heat is also enhanced but the Wilson ratio defined at low temperatures is strongly enhanced and approaches a value of 40 as $x \to x_c$.

This value of $x_c = 0.5$ is a critical value, separating a metallic and orbitally ordered phase with antiferromagnetic spin correlation ($x < x_c$) from the paramagnetic metal for $x > x_c$. As mentioned above, one observes $\theta_{cw} \approx 0$ for $x \approx x_c$. Even more remarkable is the evolution of the magnetic moment which takes a value of $S = 1/2$ as $x \to x_c$ [5,6]. This value is quite distinct from the value of $S = 1$ in Ca_2RuO_4 — the expected value for a localized Ru^{4+}-ion with 2 holes in the t_{2g}-subshell. Moreover, alloys with $x \approx x_c$ are metallic, not insulating. The explanation of this unexpected behavior presents a clear challenge.

As discussed above Sr_2RuO_4 is a good metal with an electronic structure that divides into two distinct and fractionally filled bands, a d_{xy}-band with $\approx 4/3$ electrons per Ru and the hybridized $d_{xz,yz}$-band pair with 8/3 electrons per Ru. Now the evolution with Ca substitution towards a Mott insulating state occurs because the bands are narrowed by rotation of the RuO_6 octahedra. In general, the evolution from a metal to a Mott-insulator is driven by growing Umklapp scattering. This is very clear in one dimension where studies of chains and ladders show insulating behavior at half-filling already for arbitrarily small Coulomb repulsion driven by elastic Umklapp scattering processes across the Fermi surface. Here we are dealing with an approximately two-dimensional multi-band situation. In the single-band case the Umklapp surface, across which elastic Umklapp processes are allowed, will in general be different from the Fermi surface, but at half-filling each encloses the same volume. In Sr_2RuO_4 the fractional occupancy of each subband clearly forbids elastic Umklapp scattering across the Fermi surface in low orders. Indeed this may well be the reason that Sr_2RuO_4 forms a good Landau-Fermi liquid, even though it is clearly close to a Mott insulator. One way to enhance Umklapp scattering is to transfer electrons between the subbands. This will allow low-order Umklapp scattering, when integer occupancy of the subbands is reached.

The theoretical investigation at these concentrations is inhibited by the lack of symmetry breaking at $x \approx x_c$. Therefore we cannot use the LDA+U method to build in the onsite correlations that are totally neglected in standard LDA calculations. Recently considerable progress has been achieved on the theory of the Mott transition in the Hubbard model by the use of the dynamic mean field theory (DMFT) method [11,12]. This is essentially

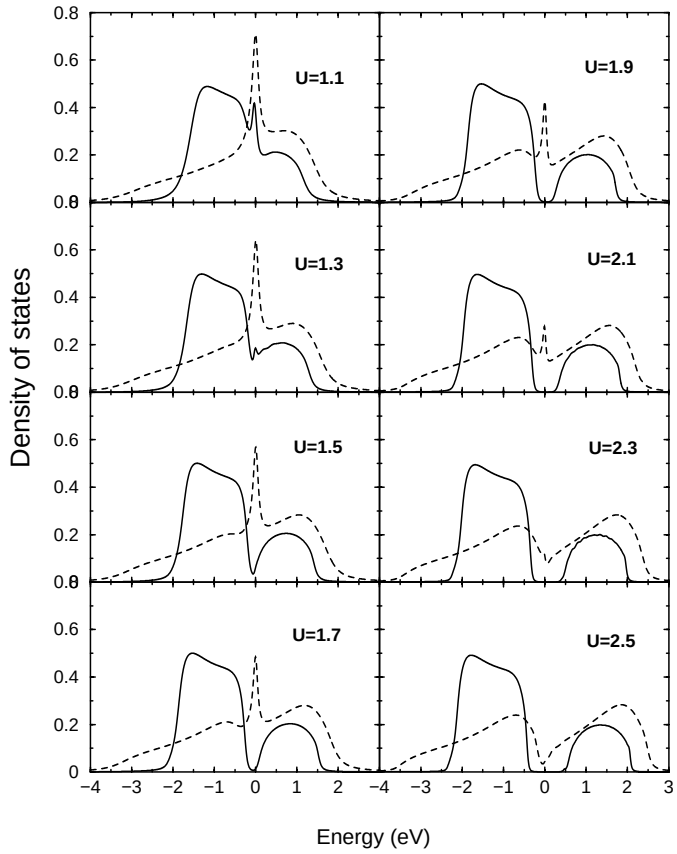

Fig. 6. Results of LDA+DMFT(NCA) calculations obtained within LDA DOS for Sr_2RuO_4. The solid line is the DOS for xz, yz-orbitals and the dashed line for (xy)-orbital. At $U = 1.5$ eV the xz, yz-orbitals become localized. At $U = 2.5$ eV additionally the localization of xy-orbital occurs. The Fermi energy is defined to be zero and was adjusted to conserve the number of particles (4 electrons per site).

an expansion around an infinite coordination number and formulates the problem in terms of an effective Anderson impurity model which is to be solved self-consistently. In this way the growth of onsite correlations can be treated as the Mott transition is approached in a paramagnetic metal. Recent advances use LDA calculations to determine the input parameters and a non-crossing approximation (NCA) to solve the effective Anderson model.

We performed a series of calculations using this LDA + DMFT (NCA) approximation scheme [26,27] for the Sr_2RuO_4 structure. We increased the value of Hubbard-U to examine how the onsite correlations grow. Figure 6 shows a series of results for the density of states (DOS) in the xy- and (xz, yz)-subbands. Since these subbands have quite different widths, the onset of Mott localization occurs at different critical values of U. Thus we see that as U is increased through a value of $U \approx 1.5$ eV there is a transfer of electrons between the subbands so that the integer occupancy of 3 electrons and Mott localization appears in (xz, yz)-subbands while the broader half-filled xy-band remains itinerant. This unusual behavior is driven by the combination of the crystal field splitting, as shown in Figure 2 ((xz, yz) lower) and the narrower bandwidth of the (xz, yz)-orbitals. A further increase in the value of U to $U \approx 2.5$ eV is required to obtain Mott localization also in the xy-subband.

These results lead us naturally to the following proposal to explain the anomalous properties in the critical concentrations $x = x_c$. The electronic configuration is now (3,1). The 3 electrons in the $\{xz, yz\}$-subbands are Mott localized and have a local moment of $S = 1/2$. The remaining valence electrons are in the itinerant xy-band and is responsible for the metallic character. Thus at this concentration we have the unusual situation of localization in only part of the 4d-orbitals and coexisting localized and itinerant 4d-orbitals. Note that in the orthorhombic crystal structure at $x = x_c$ the 2 subbands have different parity under reflection around a RuO_2-plane, similar to tetragonal Sr_2RuO_4, which forbids direct hybridization between the subbands. This proposal explains in a natural way the unexpected moment of $S = 1/2$ of the Ru-ions and the coexistence of metallic behavior and local moments.

Note that the calculations are carried out more conveniently by increasing the value of the onsite repulsion, U which however should not change appreciably with the concentration, x. In reality it is the bandwidth which is changing with the decreasing x as the RuO_6-octahedra progressively rotate when Ca is substituted for Sr. The key result however is the existence of a parameter range where this partial localization is stable. The fact that we calculated only for the highly symmetric Sr_2RuO_4 structure, rather than the distorted structure is, we believe, unimportant in establishing this (3,1) configuration as a stable electronic configuration.

3.2 Region II ($0.5 > x > 0.2$)

At lower values of x we enter Region II ($0.5 > x > 0.2$) characterized by a tilting plus rotation of RuO_6-octahedra. $Ca_{1.8}Sr_{0.2}RuO_4$ has a low-symmetry crystal structure with the space group $P2_1/c$ [28], which can be obtained from the tetragonal I4/mmm structure by rotating and tilting of the RuO_6-octahedra similar to pure Ca_2RuO_4 but with a smaller tilting angle [28] (Fig. 4c). There are now two types of in-plane oxygen ions and two types inequivalent of RuO_6-octahedra. The RuO_6-octahedra continue to be elongated in this region so that the xy-orbital continues to lie higher in energy. The metallic character of the alloys in this region shows that the itinerant character of the xy-subband is preserved, although the bandwidth will be narrowed by the additional tilting distortion of the RuO_6-octahedra. Our conclusion is that the (3,1) orbital occupation continues to hold also in Region II with localization of the electrons only in the $\{xz, yz\}$-subband.

3.3 Region I ($0.2 > x > 0$) Ca-rich

The Ca-rich region is characterized by a transition to an insulating groundstate and simultaneously a change in the crystal structure. The S-Pbca structure of the groundstate

in this region evolves continuously out the groundstate of pure Ca_2RuO_4. As discussed above, the change from elongated to compressed RuO_6-octahedra causes a switch in LDA+U in the orbital occupation numbers to (2,2) *i.e.* to a filled xy-subband and a half-filled $\{xz, yz\}$-complex. Therefore we assign the insulating groundstate in all of Region I, to an orbital occupation (2,2). The first order transition between Regions II and I as x is decreased below 0.2, is to be associated with a switch in the orbital occupation from (3,1) to (2,2).

4 Magnetic properties of the different regions

4.1 Region III

We now turn to the magnetic properties at $x \geq x_c = 0.5$. These are dominated by the local $S = 1/2$ moments. A Kondo-type of interaction between the two bands (xz, yz) and xy can be excluded due to the absence of hybridization. The xy-orbital cannot hybridize with the other two, since they have opposite parity with respect to reflection on the basal plane. *Via* Hund's rule coupling, however, an RKKY interaction between the localized spins is induced,

$$\mathcal{H}_{\mathrm{RKKY}} = -\sum_{\mathbf{q}} J_{\mathrm{H}}^2 \chi(\mathbf{q}) \mathbf{S}_{\mathbf{q}} \cdot \mathbf{S}_{-\mathbf{q}} \qquad (1)$$

where $\mathbf{S}_{\mathbf{q}} = \mathbf{S}_{yz,\mathbf{q}} + \mathbf{S}_{zx,\mathbf{q}}$ and $\chi(\mathbf{q})$ is the static spin susceptibility in the d_{xy}-band and J_{H} is the onsite Hund's rule coupling, and promotes antiferromagnetic correlations. At the same time, however, Hund's rule coupling may cause the ferromagnetic correlations through the double exchange mechanism. Thus, the two types of spin interactions mediated by the itinerant electrons of the xy-band tend to compensate each other, such that the net exchange coupling between neighboring localized spins occurs mainly through superexchange processes in the (xz, yz)-band. The highly anisotropic hopping matrix elements between these orbitals, however, leads to an essential dependence of the superexchange interaction on the orbital configuration of the minority spin electron (or single hole) of each Ru^{4+}-ion in the degenerate (xz, yz)-bands.

In order to gain more insight into the possible form of the orbital ordering we performed LDA+U calculations for the critical concentration $x_c = 0.5$. $Ca_{1.5}Sr_{0.5}RuO_4$ has the space group $I4_1/\mathrm{acd}$ [28], *i.e.* the RuO_6-octahedra are only rotated around the c-axis with no tilting (Fig. 4b). The RuO_6-octahedra remain elongated to the same degree as for pure Sr_2RuO_4 such that the xy-orbital is still higher in energy than (xz, yz)-orbitals (Fig. 2, right panel). Our calculation suggests that, under these conditions, correlation yields the orbital degeneracy in a (3,1) state. LDA+U calculations generally overestimate the stability of the Mott insulating state. In the present case we find for $U = 1.5$ eV an insulating groundstate with a charge gap also in the (xy)-subband.

Furthermore, the result of the the LDA+U calculation shows that an orbital ordering of the AFO-type is favored yielding a ferromagnetic spin exchange. The minority-spin electrons occupy alternating xz- and yz-orbitals with a slight tilting of the orbital planes away from the c-axis. This tilting indicates the partial admixture of d_{xy}-orbitals within the LDA+U approach.

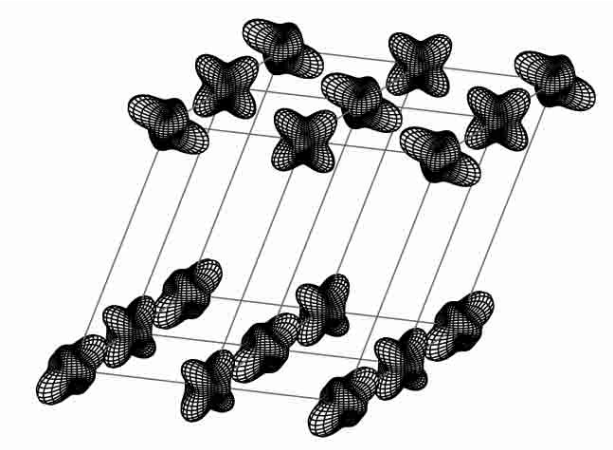

Fig. 7. Orbital ordering in $Ca_{1.8}Sr_{0.2}RuO_4$. At the figure are presented minority spin 4-d orbitals of Ru-atoms. z-axis directs upwards; x, y-axes is parallel to a bases of oxygen octahedra.

4.2 Region II

Since magnetic properties are intimately connected to the orbital order in $\{xz, yz\}$-subband, it is necessary to first examine the effect of the crystalline distortion on the orbital order. To this end we performed LDA+U calculation for this tilted structure and obtained a rather complicated orbital order. The groundstate is an AF insulator. The minority-spin electrons (1 per Ru-atom) occupy the orbitals whose planes are in average directed along the a-axis (in tetragonal notation (110) direction). However on every one of the 4 Ru-atoms in the unit cell those planes are rotated from the a-axis by $+20°$ and $+15°$ on one layer and by $-20°$ and $-15°$ on the next layer. On the average the orbital orientation corresponds to the state $d_{yz} + d_{zx}$. Also on one of the 2 Ru-atoms in every layer there is an additional tilting of the orbital plane from the long c-axis on 34° (see Fig. 7) which corresponds to the admixture of the xy-orbital component. The calculation of the easy axis using the second order perturbation theory for spin-orbit coupling gave the direction of the magnetic moment as along the a-axis (tetragonal $[1\bar{1}0]$ direction) with a 28° tilt from the layer plane (see Appendix). Measurements of the uniform magnetic susceptibility show a peak in the temperature dependence which is most pronounced for the [110] direction of the magnetic field, in agreement with our LDA+U results [3].

4.3 Region I

The orbital configuration (2,2) is non-degenerate as Hund's Rule determines a fully spin polarized $S = 1$

ionic groundstate with a single minority-spin electron in the xy-orbitals. The LDA+U method works well here and gives an AF Mott insulating groundstate.

Throughout Region I, there is a first order insulator to metal transition as the temperature is raised accompanied by a switch from compressed to elongated RuO_6-octahedra. It is tempting to interpret this as a first order transition between the orbital occupancies from (2,2) to (3,1). However a detailed examination of this proposal has not been made. In this context it would be also interesting to study the effect of pressure. Since the low-temperature phase of Ca_2RuO_4 has larger volume than the high-temperature phase (see Tab. 1), pressure tends to stabilize the latter. Assuming that indeed the (3,1) electronic distribution is realized in this structural state, then a orbitally ordered phase accompanied by magnetic order based on the localized spin-1/2 degree of freedom could be realized at low enough temperature. Since the crystal structure is close to the one at $x = 0.2$ (see Tab. 1) one might conclude that AF order would prevail. However, as we will see in the next section, the final form of the exchange interactions between the spins is a subtle issue, in particular, if a staggered orbital component are included.

5 Effective model for the (3,1) electron distribution

5.1 Derivation of spin-isospin Hamiltonian

In this section we derive the effective Hamiltonian for the localized spin and orbital degrees of freedom in the electron configuration $(n_{(\alpha,\beta)}, n_\gamma) = (3, 1)$ which covers the boundary of region II and III and all of region II. The electrons in the d_{yz}- and d_{zx}-orbital are localized, while the γ-band remains metallic, although it is half-filled. We ignore here this metallic band and concentrate on the localized degrees of freedom. The single hole occupying the two localized orbitals has a spin-1/2 and orbital index. The latter can be described as isospin-1/2 using the notation $|+\rangle$ for the d_{yz}- and $|-\rangle$ for the d_{zx}-orbital. The isospin operator $\boldsymbol{I}$ acts on these states by $I^z|\pm\rangle = \pm\frac{1}{2}|\pm\rangle$ and is a generator of an SU(2) transformation in orbital space.

We will concentrate on the strongest interaction between the localized degrees of freedom. The nearest-neighbor hopping due to π-hybridization between the Ru-d and O-p-orbitals lead to the formation of two independent quasi-one-dimensional bands, with dispersion in y (x)-direction for the d_{yz} (d_{zx})-orbital. Including the onsite interactions the Hamiltonian for these two orbitals has the form

$$\begin{aligned}\mathcal{H} = &-t\sum_{i,\mathbf{a},s}(c^\dagger_{i+a_x,-,s}c_{i,-,s} + c^\dagger_{i+a_y,+,s}c_{i,+,s} + \text{h.c.})\\ &+U\sum_{i,\mu=+,-} n_{i,\mu,\uparrow}n_{i,\mu,\downarrow} + U'\sum_i n_{i,+,s}n_{i,-,s'}\\ &-2J_{\rm H}\sum_i(\mathbf{S}_{i,+}\cdot\mathbf{S}_{i,-} + \frac{1}{4}n_{i,+}n_{i,-}) \qquad (2)\end{aligned}$$

where t denotes the hopping matrix element, U and U' are the onsite intra- and interorbital Coulomb repulsion and $J_{\rm H}$ is the Hund's rule coupling (the vector $\mathbf{a} = (1, 0)$ and $(0, 1)$ connects the nearest neighbor sites). We can reduce the number of parameters by the relation $U = U' + 2J_{\rm H}$.

We now consider the case of a nearest-neighbor bond along the x-direction and calculation the effective spin-spin interaction for different orbital configurations. For illustration of the processes involved we introduce the following self-explanatory notation shown in the two examples,

$$|+,\uparrow\rangle_i \otimes |+,\downarrow\rangle_{i+a_x} = \left|\begin{matrix}\uparrow & \downarrow\\ \uparrow\downarrow & \uparrow\downarrow\end{matrix}\right\rangle \qquad (3)$$

$$|+,\uparrow\rangle_i \otimes |-,\uparrow\rangle_{i+a_x} = \left|\begin{matrix}\uparrow & \uparrow\downarrow\\ \uparrow\downarrow & \uparrow\end{matrix}\right\rangle. \qquad (4)$$

The upper (lower) row in the isospinor notation correspond to the d_{yz} (d_{zx})-orbital. Now we discuss the virtual exchange processes leading to the spin interactions for the x-bond.

(1) The configuration $|+, s\rangle \otimes |+, s'\rangle$ does not lead to any interaction. (2) The configuration $|-, s\rangle \otimes |-, s'\rangle$ yields antiferromagnetic superexchange through the exchange path,

$$\left|\begin{matrix}\uparrow\downarrow & \uparrow\downarrow\\ \uparrow & \downarrow\end{matrix}\right\rangle \stackrel{-t}{\rightarrow} \left|\begin{matrix}\uparrow\downarrow & \uparrow\downarrow\\ 0 & \uparrow\downarrow\end{matrix}\right\rangle \stackrel{-t}{\rightarrow} \left|\begin{matrix}\uparrow\downarrow & \uparrow\downarrow\\ \downarrow & \uparrow\end{matrix}\right\rangle. \qquad (5)$$

This leads to an effective Hamiltonian

$$\mathcal{H}' = J\left(\mathbf{S}_i\cdot\mathbf{S}_{i+a_x} - \frac{1}{4}\right) \qquad (6)$$

with an exchange coupling constant

$$J = \frac{4t^2}{U}\cdot \qquad (7)$$

(3) Finally the configuration $|+, s\rangle \otimes |-, s'\rangle$ gives an ferromagnetic spin coupling by the following type of path,

$$\left|\begin{matrix}\uparrow & \uparrow\downarrow\\ \uparrow\downarrow & \uparrow\end{matrix}\right\rangle \stackrel{-t}{\rightarrow} \left|\begin{matrix}\uparrow & \uparrow\downarrow\\ \uparrow & \uparrow\downarrow\end{matrix}\right\rangle \stackrel{-t}{\rightarrow} \left|\begin{matrix}\uparrow & \uparrow\downarrow\\ \uparrow\downarrow & \uparrow\end{matrix}\right\rangle. \qquad (8)$$

Here the intermediate state has lower energy, if the two spins are in a triplet configuration due to the Hund's rule coupling. The interaction energies for the intermediate states corresponding to the spin singlet and triplet state are

$$\Delta E_{\rm singlet} = U' + J_{\rm H} \qquad (9)$$

$$\Delta E_{\rm triplet} = U' - J_{\rm H} \qquad (10)$$

so that the effective Hamiltonian can be cast into the form

$$\mathcal{H}'' = J'\left(\mathbf{S}_i\cdot\mathbf{S}_{i+a_x} + \frac{1+\alpha}{2(1-\alpha)}\right) \qquad (11)$$

with

$$J' = -\frac{2t^2J_{\rm H}}{U'^2 - J_{\rm H}^2} = -J\frac{1-\alpha}{(3\alpha-1)(\alpha+1)} \qquad (12)$$

where $\alpha = U'/U < 1$. Note that α should be sufficiently larger than $1/3$ in order that the second-order perturbation approach is valid and the electron distribution (3,1) is unique. The orbital configurations in the basis of $|+\rangle$ and $|-\rangle$ are not affected in this second order perturbation scheme. Therefore the effective isospin Hamiltonian is Ising-like.

Turning to the bond along the y-axis we need only to exchange the role of the two orbitals (d_{yz} and d_{zx}) and obtain the same result. Therefore we can write the complete effective Hamiltonian for the localized degrees of freedom as,

$$\mathcal{H} = J \sum_{i,\mathbf{a}} \left[\left\{ A(I^z_{i+\mathbf{a}} + \eta_{\mathbf{a}})(I^z_i + \eta_{\mathbf{a}}) + B \right\} \mathbf{S}_{i+\mathbf{a}} \cdot \mathbf{S}_i \right. \\ \left. + [C(I^z_{i+\mathbf{a}} + \eta'_{\mathbf{a}})(I^z_i + \eta'_{\mathbf{a}}) + D] \right] \quad (13)$$

where the coefficients are given by

$$A = \frac{3\alpha^2 + 1}{(3\alpha - 1)(\alpha + 1)} \quad (14)$$

$$B = \frac{-(1-\alpha)^2}{(3\alpha^2 + 1)(3\alpha - 1)(\alpha + 1)} \quad (15)$$

$$C = \frac{5 - 3\alpha}{4(3\alpha - 1)} \quad (16)$$

$$D = \frac{1}{(5 - 3\alpha)(3\alpha - 1)} \quad (17)$$

$$\eta_{\mathbf{a}} = -\frac{(3\alpha - 1)(\alpha + 1)}{2(3\alpha^2 + 1)}(a_x^2 - a_y^2) \quad (18)$$

$$\eta'_{\mathbf{a}} = -\frac{3\alpha - 1}{2(5 - 3\alpha)}(a_x^2 - a_y^2). \quad (19)$$

Note that the coefficients $\eta_{\mathbf{a}}$ and $\eta'_{\mathbf{a}}$ have opposite sign for the x- and y-axis bonds.

Lattice distortions breaking the tetragonal symmetry yield a bias for the local orbital configuration. For the two basic orthorhombic distortions, described by the lattice strain combinations $\epsilon_1 = \epsilon_{xx} - \epsilon_{yy}$ and $\epsilon_2 = \epsilon_{xy}$ (tetragonal notation), we can add the following coupling terms to the Hamiltonian,

$$\mathcal{H}_{\rm dist} = \sum_i [K_1 \epsilon_1 I^z_i + K_2 \epsilon_2 I^x_i] \quad (20)$$

where K_1 and K_2 are coupling constants. Note that the first term corresponds to a uniform field parallel to the z-axis of the isospin, while the second is a transverse field. Both drive a ferro-orbital correlation.

5.2 Mean field discussion

We analyze now the properties of our effective model by means of mean field theory ignoring fluctuations and the influence of the itinerant xy-band. This discussion shows that the main features of the different phases where the electron distribution (3,1) is applicable are indeed described well within our reduced effective model. A discussion beyond the mean field level will be given elsewhere.

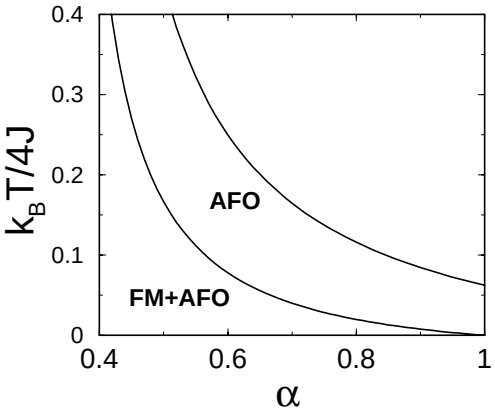

Fig. 8. Mean field phase diagram temperature *versus* $\alpha = U'/U$ for $x = 0.5$.

5.2.1 Tetragonal system

The analysis of the parameters of the effective Hamiltonian shows that a higher energy scale is associated with the isospins. Their basic interaction is of Ising-AFO-type, because $C > 0$ for all α in the proper range. As a consequence the spins correlate ferromagnetically at a lower energy scale. Hence, we will decouple the effective Hamiltonian for the spin and isospin with mean values,

$$m_I = \langle I^z_i \rangle \quad \text{and} \quad s = \langle S^z_i \rangle \quad (21)$$

where m_I is staggered with opposite sign on the two sublattices and s is uniform. The coupled self-consistent equations are obtained readily,

$$m_I = \frac{\sum_{r=\pm 1} r \mathrm{e}^{\beta C r m_I} \cosh\left(\beta \left(A\left(\eta^2_{\mathbf{a}} - \frac{r m_I}{2}\right) + B\right) s\right)}{2 \sum_{r=\pm 1} \mathrm{e}^{\beta C r m_I} \cosh\left(\beta \left(A\left(\eta^2_{\mathbf{a}} - \frac{r m_I}{2}\right) + B\right) s\right)} \quad (22)$$

$$s = \frac{\sum_{r=\pm 1} \mathrm{e}^{\beta C r m_I} \sinh\left(\beta \left(A\left(\eta^2_{\mathbf{a}} - \frac{r m_I}{2}\right) + B\right) s\right)}{2 \sum_{r=\pm 1} \mathrm{e}^{\beta C r m_I} \cosh\left(\beta \left(A\left(\eta^2_{\mathbf{a}} - \frac{r m_I}{2}\right) + B\right) s\right)} \quad (23)$$

where $\beta = J/2k_{\rm B}T$ is the inverse temperature in units of the exchange energy J. The isospin order has the higher transition temperature T_0 determined by the equation

$$k_{\rm B} T_0 = \frac{CJ}{4} \cdot \quad (24)$$

The onset of FM order occurs at much lower temperature so that it is justified to consider m_I as already saturated, $m_I = 1/2$. Then Curie-temperature for the spin is given by

$$k_{\rm B} T_{\rm C} = -\frac{J}{4}\left[A\left(\eta^2_{\mathbf{a}} - \frac{1}{4}\right) + B\right]. \quad (25)$$

In Figure 8 we show the phase diagram of temperature *versus* the parameter $\alpha = U'/U$ which determines the coupling constants. The tendency towards FM order is in good agreement with the LDA+U result for $x = 0.5$, apart from the fact that the contributions of xy-orbital have been ignored. This analysis suggests that the orbital order is governed by the exchange processes included in our Hamiltonian.

5.2.2 Crystal distortion

Let us now consider the influence of a spontaneous crystal deformation which characterizes region II ($0.2 < x < 0.5$). We will not discuss the origin of the distortion, but take it as given with a strength which depends on x. The FO bias introduced by a uniform lattice distortion is in competition with the AFO exchange interaction. In particular, a finite strain ϵ_2 would introduce a transverse field in the effective Ising Hamiltonian for orbital interactions. An Ising-model in a transverse field has a quantum critical point beyond which the AFO order would be suppressed for any temperature.

We consider here the general case where both ϵ_1 and ϵ_2 are finite, as realized in Region II. We distinguish now between the two sublattices A and B on the square lattice and assign different mean fields to them. Analogous to the case above we may separate the spin and the isospin problem. First we consider the isospin problem in the absence of spin correlation. The corresponding self-consistent equations have the form,

$$m_{IA} = f(\beta, m_{IB}) \quad \text{and} \quad m_{IB} = f(\beta, m_{IA}) \tag{26}$$

with

$$f(\beta, m) = -\frac{2JCm + K_1\epsilon_1}{2\sqrt{(2JCm + K_1\epsilon_1)^2 + K_2^2\epsilon_2^2}} \times \tanh\left(\beta\sqrt{(2JCm + K_1\epsilon_1)^2 + K_2^2\epsilon_2^2}\right). \tag{27}$$

It is easy to verify from this set of equations that for finite crystal distortion there is a uniform component $m = (m_{IA} + m_{IB})/2$ at all temperatures and that the staggered moment $m_I = (m_{IA} - m_{IB})/2$ occurs only at low temperature or not at all, depending on which side of the quantum critical point the system lies. Hence the staggered moment may play a minor role on the background of the uniform FO orbital arrangement.

In Figure 9 the numerical solution of equations (26, 27) is shown for $\alpha = 0.75$ assuming that both ϵ_1 and ϵ_2 are finite with a ratio $K_1\epsilon_1/K_2\epsilon_2 = 3/2$. Turning $\epsilon_{1,2}$ gradually on we observe that the staggered AFO component is diminished in favor of the FO arrangement (Fig. 9a) with a critical point where the staggered component completely vanishes. Figure 9b shows the orbital orientation on the two sublattices $|d\rangle_{A,B} = \cos\phi_{A,B}|+\rangle + \sin\phi_{A,B}|-\rangle$. Obviously, very close to the quantum critical point we find a dominant FO arrangement with a weak staggered component. This describes qualitatively the favored ordering pattern in the LDA+U calculation for $x = 0.2$, where in each layer the orbital plane has an alternating orientation of 20° and 15° with respect to the [110] (FO) direction. The comparison with our mean field data suggests that the system is then rather close to the quantum critical point.

Assuming again that at the energy scale where spin correlation sets in the orbital pattern is basically established, we draw the diagram of transition temperature

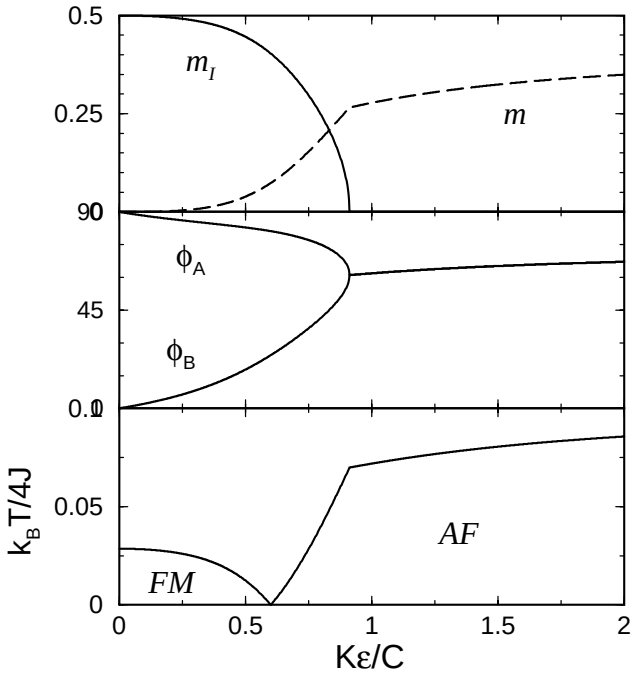

Fig. 9. Effect of lattice deformation $K_1\epsilon_1 = 1.5K_2\epsilon_2 = K\epsilon$ on the orbital order and the effective spin exchange ($\alpha = 0.75$). Top: Staggered orbital moment m_I and uniform orbital moment m; Middle: Orientation of the orbital plane $\cos\phi|+\rangle + \sin\phi|-\rangle$ for the sublattices A and B; Bottom: effective spin exchange ferromagnetic and antiferromagnetic.

versus the strain in Figure 9c. Then we analyze the spin correlation fixing the orbital order by the $T = 0$-solution of equations (26, 27). This is again justified by the observation that the isospin mean field has saturated at the temperature when spin order sets in. We find weak ferromagnetic coupling for small distortion and stronger antiferromagnetic coupling for larger distortion. The crossover in the spin interaction is still in the region of rather strong staggered orbital correlations. Note that the crossover point between FM and AF spin exchange depends on α and move towards larger $K\epsilon$ for smaller α.

Guided by this phase diagram we may interpret the region II in terms of increasing strain as we progress from $x = 0.5$ to 0.2. At $x = 0.2$ the quantum critical point has been approached but not passed. This interpretation is entirely based on the localized orbitals of the α-β-bands. From the LDA+U calculation we conclude, however, that the γ -band is also involved in the spin correlations, as is seen in the tilting of the orbital plane away from the z-axis for the minority spins. As mentioned earlier the γ-band should introduce an RKKY-interaction *via* the Hund's rule coupling, which is most likely antiferromagnetic, thus further diminishing the FM correlation.

An interesting feature occurs in our effective model in connection with the sign change of the spin exchange interaction as mentioned above. $Ca_{2-x}Sr_xRuO_4$ as a random alloy does not provide a uniform crystal deformation, but the strain depends on the local Sr and Ca distribution around each Ru-ion. Thus, in the regime of switching

Table 2. Regions of $Ca_{2-x}Sr_xRuO_4$ with orbital occupancy, localized orbital and spin degrees of freedom and order or (dominant correlations) (AF = spin antiferromagnetic, FM = spin ferromagnetic, AFO = antiferro-orbital, FO = ferro-orbital).

Region	$(n_{yz,zx}, n_{xy})$	orbital	spin	order (correlation)
I ($0 \leq x < 0.2$)	(2,2)	–	$S = 1$	AF
II ($0.2 \leq x < 0.5$)	(3,1)	(yz, zx)	$S = \frac{1}{2}$	FO, (AF)
III ($x \to 0.5$)	$(3, 1)$	(yz, zx)	$S \to \frac{1}{2}$	(AFO) , (FM)
III ($x = 2$)	$\left(\frac{8}{3}, \frac{4}{3}\right)$	–	S=0	–

between FM and AF coupling, this can lead to frustration effects at low temperature. Recent experimental data indicate indeed a glass-like behavior [30].

6 Discussion

We have presented a consistent picture for the unusual phases of the isoelectronic alloy series $Ca_{2-x}Sr_2RuO_4$ based on the full multi-band electronic structure (see Tab. 2). Starting from the good metal Sr_2RuO_4, we find the effect of Ca-substitution is to transfer electrons from the wider xy-band to the narrower (xz, yz) bands until at a critical value of $x_c = 0.5$ there is integer occupancy of both subbands. The progressive rotation of the RuO_6 octahedra in this region leads to Mott localization of the 3 electrons in the narrower (xz, yz) bands while the wider xy-band which is now half-filled, remains metallic. This partial localization of the $4d$ electrons can explain the puzzling observation of the coexistence of free $S = 1/2$ local moments and metallic behavior in $Ca_{1.5}Sr_{0.5}RuO_4$. The actual metal to insulator transition occurs between the Ca-rich Regions I ($0 \leq x < 0.2$) and II ($0.2 \leq x < 0.5$). We interpret this transition as driven by a change in the orbital occupancy to a completely filled xy-band leaving 2 electrons in the localized (xz, yz) bands. In this case the ordered local spin has the conventional value, $S = 1$, whereas in the metallic Region II short-range correlations of a local $S = 1/2$ spin combined with orbital order are realized, generating a pronounced anisotropy in the magnetic response.

One of the curious aspects of Region II is the fact that the half-filled xy-orbital remains itinerant. It is not easy to test experimentally which among the bands is really responsible for the metallic behavior. The basic feature of the state we propose is the presence of a single Fermi surface of electron-like character in the xy- or γ-sheet. One method which might be able to probe this proposal is angle-resolved photo emission spectroscopy (ARPES).

Recently the electronic structure and magnetic properties of $Ca_{2-x}Sr_2RuO_4$ have also been investigated by LSDA calculations [29]. The authors have concluded that the crystal structure distortions (rotation, tilt and compression of the O-octahedra) when Ca is substituted for Sr lead to a narrowing and shifting of the bands and hence to the enhancement of ferro- and antiferromagnetic instabilities. However these calculations do not include the effects of onsite Coulomb interactions between d-electrons which are responsible for the suppression of charge fluctuations and for the Mott metal-insulator transition as Ca_2RuO_4 is approached.

We would like to thank Y. Maeno, S. Nakatsuji, T. Nomura, M. Braden, D. Vollhardt, T. Pruschke, M. Zölfl, J. Schmalian and A. Poteryaev for many helpful discussions. This work was financially supported by the Russian Foundation for Basis Research grant RFFI-01-02-17063, a Grant-in-Aid of the Ministry of Education, Science, Sports and Culture of Japan (No. 12046238), Netherland Organization for the Advance of Pure Science (NWO 047-008-012), the Sonderforschungsbereich 484 of the Deutsche Forschungsgemeinschaft and the Swiss Nationalfonds.

Appendix A: Effect of spin-orbit coupling

For the Ru $4d$-t_{2g}-orbitals spin-orbit coupling plays an important role. If we restrict to the three t_{2g}-orbitals, the onsite spin-orbit coupling Hamiltonian can is given by

$$\mathcal{H}_{\mathrm{s-o}} = \lambda \sum_i \sum_{a,b,c} \sum_{s,s'} \epsilon_{abc} c^\dagger_{ia,s} \sigma^c_{ss'} c_{ib,s'} \qquad \text{(A.1)}$$

where λ is the coupling constant and ϵ_{abc} the completely antisymmetric tensor (a, b, $c = \{x, y, z\}$). We identify the indices x, y and z with the orbitals d_{yz}, d_{zx} and d_{xy}, respectively.

In the framework of LDA+U calculation the easy axis direction was calculated via minimizing the energy of spin-orbit coupling in the second order perturbation theory as a function of Euler angles (α, β, γ) defining the direction of magnetization:

$$E(\alpha, \beta, \gamma) = \sum_{\boldsymbol{k}} \sum_{n\sigma, n'\sigma'} \frac{f_{n\sigma\boldsymbol{k}} - f_{n'\sigma'\boldsymbol{k}}}{E_{n\sigma}(\boldsymbol{k}) - E_{n'\sigma'}(\boldsymbol{k})} |\langle \Psi^{\boldsymbol{k}}_{n\sigma} | \hat{\mathbf{l}} \cdot \hat{\mathbf{s}}' | \Psi^{\boldsymbol{k}}_{n'\sigma'} \rangle|^2, \qquad \text{(A.2)}$$

$$\hat{\mathbf{l}} \cdot \hat{\mathbf{s}'} = \sum_\mu \hat{l}_\mu \cdot \hat{s'}_\mu = \sum_{\mu\nu} \hat{l}_\mu \cdot U_{\mu\nu}(\alpha, \beta, \gamma) \hat{s}_\nu \qquad \text{(A.3)}$$

where $E_{n\sigma}(\boldsymbol{k})$ is the energy of nth band for spin projection σ at point $\boldsymbol{k}$ in the Brillouin zone, $f_{n\sigma\boldsymbol{k}}$ is equal 1 if the corresponding band is occupied (its energy is below the Fermi level) and is equal 0 in the opposite case. $\Psi^{\boldsymbol{k}}_{n'\sigma'}$ is the Bloch wave function, $\hat{l}_\mu$ and $\hat{s}_\nu$ are components of vector operators of orbital and spin moments, $U_{\mu\nu}(\alpha, \beta, \gamma)$ is transformation matrix for rotation of a vector for Euler angles (α, β, γ).

References

1. Y. Maeno , H. Hashimoto, K.Yoshida, S. Nishizaki, T. Fujita, J.G. Bednorz, F. Lichtenberg, Nature (London) **372**, 532 (1994).
2. Y. Maeno, T.M. Rice, M. Sigrist, Physics Today **54**, 42 (2001).
3. S. Nakatsuji, Y. Maeno, Phys. Rev. Lett. **84**, 2666 (2000).
4. S. Nakatsuji, S. Ikeda, Y. Maeno, J. Phys. Soc. Jpn **66**, 1868 (1997).
5. S. Nakatsuji, Y. Maeno, Phys. Rev. B **62**, 6458 (2000).
6. S. Nakatsuji, Ph.D. Thesis, Kyoto University (2000).
7. A.P. Mackenzie, S.R. Julian, A.J. Diver, G.J. McMullan, M.P. Ray, G.G. Lonzarich, Y. Maeno, S. Nishizaki, T. Fujita, Phys. Rev. Lett. **76**, 3786 (1996).
8. T. Oguchi, Phys. Rev. B **51**, 1385 (1995); D.J. Singh, Phys. Rev. B **52**, 1358 (1995).
9. V.I. Anisimov, J. Zaanen, O.K. Andersen, Phys. Rev. B **44**, 943 (1991).
10. D. Vollhardt, in *Correlated Electron Systems*, edited by V.J. Emery (World Scientific, Singapore, 1993), p. 57.
11. Th. Pruschke, M. Jarrell, J.K. Freericks, Adv. Phys. **44**, 187 (1995).
12. A. Georges, G. Kotliar, W. Krauth, M.J. Rozenberg, Rev. Mod. Phys. **68**, 13 (1996).
13. I.A. Nekrasov, K. Held, N. Blümer, A.I. Poteryaev, V.I. Anisimov, D. Vollhardt, Euro Phys. J. B **18**, 55 (2000).
14. K. Held, I.A. Nekrasov, N. Blümer, V.I. Anisimov, D. Vollhardt, Int. J. Mod. Phys. B **15**, 2611 (2001).
15. Th. Pruschke, N. Grewe, Z. Phys. B **74**, 439 (1989).
16. V.I. Anisimov, I.A. Nekrasov, D.E. Kondakov, T.M. Rice, M. Sigrist, `cond-mat/0011460`.
17. A.P. Mackenzie, S.R. Julian, A.J. Diver, G.J. McMullan, M.P. Ray, G.G. Lonzarich, Y. Maeno, S. Nishizaki, T. Fujita, Phys. Rev. Lett. **76**, 3786 (1996).
18. Y. Maeno, K. Yoshida, H. Hashimoto, S. Nishizaki, S. Ikeada, M. Nohara, T. Fujita, A.P. Mackenzie, N.E. Hussey, J.G. Bednorz, F. Lichtenberg, J. Phys. Soc. Jpn **66**, 1405 (1997).
19. M. Braden, G. Andre, S. Nakatsuji, Y. Maeno, Phys. Rev. B **58**, 847 (1998).
20. M. Braden, H. Moudden, S. Nishizaki, Y. Maeno, T. Fujita, Physica C **273**, 248 (1997).
21. T. Katsufuji *et al.*, Phys. Rev. Lett. **76**, 26 (1996).
22. A.V. Puchkov, Z.-X. Shen, T. Kimura, Y. Tokura, Phys. Rev. B **58**, R13322 (1998).
23. V.I. Anisimov, F. Aryasetiawan, A.I. Lichtenstein, J. Phys. Cond. Matt. **9**, 767 (1997).
24. A.V. Puchkov, M.C. Schabel, D.N. Basov, T. Startseva, G. Gao, T. Timusk, Z.-X. Shen, Phys. Rev. Lett. **81**, 2747 (1998).
25. G. Cao, S. McCall, J.E. Crow, R.P. Guertin, Phys. Rev. Lett. **78**, 1571 (1997).
26. M.B. Zölfl, Th. Pruschke, J. Keller, A.I. Poteryaev, I.A. Nekrasov, V.I. Anisimov, Phys. Rev. B **61**, 12810 (2000).
27. M.B. Zölfl, I.A. Nekrasov, Th. Pruschke, V.I. Anisimov, J. Keller, Phys. Rev. Lett. **87**, 276403 (2001).
28. O. Friedt, M. Braden, G. André., P. Adelmann, S. Nakatsuji, Y. Maeno, Phys. Rev. B **63**, 174432 (2001).
29. Z. Fang, K. Terakura, Phys. Rev. B **64**, 020509 (2001).
30. S. Nakatsuji, K. Sugahara (private communication).